Conductive Molecular Crystals. Structural, Electrical, and Magnetic Properties of Partially Oxidized Octamethyltetrabenzporphyrinatonickel(II)

Terry E. Phillips, Raymond P. Scaringe, Brian M. Hoffman,* and James A. Ibers*

Contribution from the Department of Chemistry and Materials Research Center, Northwestern University, Evanston, Illinois 60201. *Received March 26, 1979*

Abstract: Oxidation of 1,4,5,8,9,12,13,16-octamethyltetrabenzporphyrinatonickel(II), Ni(OMTBP), by elemental iodine yields two distinct complexes, Ni(OMTBP)$(I_3)_\rho$, where ρ = 0.36 and 0.97. The two complexes were characterized by resonance Raman and EPR spectroscopy and by static magnetic susceptibility and four-probe electrical conductivity measurements. Additionally the crystal and molecular structure of the ρ = 0.36 complex was determined from a study of both ordinary and diffuse X-ray scattering. The compound Ni(OMTBP)$(I_3)_{0.36}$ crystallizes in space group D_{4h}^{11}-$P4_2/nbc$ of the tetragonal system with four formula units in a cell of dimensions a = 21.011 (9) Å and c = 7.556 (6) Å. The structure solution, the first for a tetrabenzporphyrin, was obtained by standard methods and refined to a conventional R index of 0.050, based on 687 significant observations. The predominant feature of the crystal structure is columns of S_4 ruffled macrocycles stacked with large intermolecular spacings along the c axis. Chains of severely disordered linear I_3^- units parallel the stacking axis, between adjacent macrocycle columns. g values are near the free electron value and indicate that the unpaired spin density is ligand, not metal based; closer analysis reveals a minor contribution from the iodide chain. The symmetry of the g and line-width tensors indicates that in the ρ = 0.97 material the macrocycles also stack along c with the linear I_3^- ions paralleling this axis. The magnetic susceptibility of the ρ = 0.36 crystals is Curie-like, indicating negligible interactions between spins. The more highly oxidized ρ = 0.97 material exhibits a small but noticeable coupling between spins ($J < 50$ cm^{-1}). The temperature-dependent electrical conductivity of each material exhibits qualitatively the same response: an activated conductivity occurs at temperatures less than a value T_m; above T_m the conductivity decreases in a metal-like manner from the maximum σ_m. Values of T_m and σ_m for the ρ = 0.36 and 0.97 complexes are respectively 300 K, 12 S cm^{-1} and 340 K, 3 S cm^{-1}. The existence of high conductivity but large intrastack spacings emphasizes the importance of partial oxidation in achieving high conductivity in a molecular crystal. This well-documented combination of a metal-like conductivity but a Curie-law susceptibility is unprecedented, and is discussed in terms of intuitive models of charge transport in molecular crystals.

Introduction

Intensive efforts over the past decade have been directed toward the preparation of highly conducting molecular crystals with coordination complexes as the fundamental units.[1] The conductive crystals which have been studied to date are of two classes. The most widely known systems, exemplified by the tetracyanoplatinate salts, are those in which the transport properties can be understood almost completely in terms of carriers confined to a conducting spine of metal atoms. The coordinated ligands (e.g., CN^-), although essential for defining the properties of the molecule or ion, play little or no direct part in the charge-transport process. Quite recently, however, we have prepared a variety of conducting systems whose transport properties are largely ligand based.[2,3] The metal ion acts in a decisive manner to modify the ligand properties, but the transport process does not appear directly to involve the metal.

Work on systems with metal-centered conduction, as well as on organic molecular metals, indicated that two desirable, if not indeed necessary, criteria for creating a conductive molecular crystal are (1) that the parent compound be a planar complex of metal and ligand and (2) that the complex be made to adopt a nonintegral oxidation state.[1a] This last criterion has typically been met by a partial oxidation of a complex of integral oxidation state, but in principle it could equally well be met by a partial reduction.

We have shown that it is possible to oxidize partially a wide variety of metal-ligand complexes in which L is a variant on the porphin skeleton.[2,3] We have taken advantage of the chemical flexibility offered by variations in the ligand framework and the incorporated metal. Elemental I_2 has proved to be our most successful oxidant, probably because it forms a number of reduced species (I^-, I_3^-, I_5^-) which all have approximately the same volume per iodine atom. This, in effect allows the metal-ligand system freedom to adopt whatever degree of partial oxidation is most favored in the particular material. Furthermore, the state of the iodine, and thus the degree of oxidation, is readily identified by spectroscopic means[4] and diffraction techniques.[5]

In this paper we present a complete study of the structural, magnetic, and charge-transport properties of a pair of materials derived from the partial oxidation with iodine of the planar metal-ligand system 1,4,5,8,9,12,13,16-octamethyltetrabenzporphyrinatonickel(II), herein abbreviated Ni(OMTBP).[6]

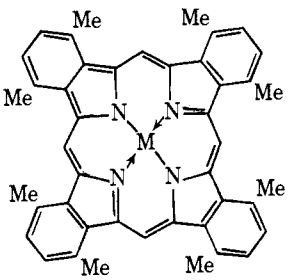

The two conductive materials discussed here have very different stoichiometries, Ni(OMTBP)I_x, with $x = 1.08 \pm 0.01$ and 2.9 ± 0.3, and thus represent the only case to date in which crystals of a given metallomacrocycle have been isolated at different levels of partial oxidation. The crystal structure for x = 1.08 is the first involving tetrabenzporphyrin and exhibits columns of ruffled macrocycles with large intermolecular spacings. The iodine occurs as I_3^- chains which parallel the macrocyclic columns, and which exhibit an interesting one-dimensional disorder. Both materials have metal-like conductivities at or above room temperature, but exhibit Curie or nearly Curie law susceptibilties.

Existence of high conductivity but large intrastack spacing in these crystals emphasizes the importance of partial oxidation in achieving a conductive molecular crystal. The combination of a metal-like conductivity with a Curie-like susceptibility is

0002-7863/80/1502-3435$01.00/0

in contrast with ordinary pictures of the conducting state. Instead, the results are in surprisingly good accord with an intuitive picture of diffusive, or hopping, "electron-holes" as carriers.

Experimental Section

Syntheses. The Ni(OMTBP) macrocycle was prepared by a condensation reaction[7] of 1,3,4,7-tetramethylisoindole[8] and a threefold molar excess of nickel acetate tetrahydrate in refluxing 1,2,4-trichlorobenzene under N_2. When the reaction mixture was cooled, crude product precipitated. This product was purified by recrystallization from 1,2,4-trichlorobenzene to yield lustrous purple crystals. The yield, based on 1,3,4,7-tetramethylisoindole, ranged from 28 to 35%.

Oxidation of Ni(OMTBP) by I_2 in 1,2,4-trichlorobenzene[3] yields needlelike crystals of stoichiometry $Ni(OMTBP)I_{1.08\pm0.01}$.[9] The crystals are dark purple-pink by reflected light. When Ni(OMTBP) is oxidized by I_2 in chlorobenzene, thin, bronze needles are obtained in addition to $Ni(OMTBP)I_{1.08}$. These analyze as $Ni(OMTBP)I_{2.9\pm0.3}$. The relative proportion of the two materials varies and appears to depend on the solvent and crystal-growth conditions, with the $Ni(OMTBP)I_{1.08}$ always predominating.

Anal. Calcd for $Ni(OMTBP)I_{1.08}$: C, 64.7; H, 4.44; N, 6.86. Found: C, 65.0; H, 4.05; N, 6.85. Calcd for $Ni(OMTBP)I_{2.9}$: C, 50.45; H, 3.46; N, 5.35. Found: C, 50.45; H, 2.91; N, 5.10.

Resonance Raman Measurements. The resonance Raman measurements were performed at ambient temperature on samples contained in spinning, 5-mm Pyrex tubes. The excitation source was the 5145-Å line of an Ar^+-ion laser. The spectrometer, built by Professor D. Shriver, operates in a 180° backscattering geometry and is described elsewhere.[10] The raw data were corrected for base line, background, and, where needed, plasma lines.

Magnetic Measurements. The static susceptibility, χ, was measured by the Faraday technique using $Hg(Co(SCN)_4)$ as a standard. EPR spectra were obtained on a modified Varian E-4 spectrometer with a 9-in. Varian magnet (no. 2500). The cavity resonance frequency was measured to an accuracy of 4 ppm by a transfer oscillator technique. The magnetic field was calibrated with DPPH (g = 2.0036) and Fremy's salt (g = 2.0055; a^N = 13.0 G). Single-crystal data were taken by using silicone grease to mount the sample crystal on a Teflon holder attached to a quartz rod. This in turn was inserted in a goniometer of standard design mounted firmly to the cylindrical microwave cavity (Varian no. 4533). The goniometer could be set to a precision of 0.01 rad. Temperature-dependent EPR measurements were performed in an Air Products LTD-3-110 system. The temperature, stable to better than ±1K, was monitored by a calibrated chromel Fe-Au thermocouple placed in the immediate vicinity of the sample.

For EPR intensity measurements, the incident microwave power was set at −20 dB from the power level where saturation effects were first observable. The amplitude of the modulation field was maintained at 10-20% of the signal line width. The EPR line shape for single crystals of $Ni(OMTBP)I_{1.08}$ remains unchanged between 300 and 20 K. Throughout this range, relative intensities of the EPR signal were taken to be proportional to Γ^2P, where Γ is the peak-to-peak line width of the first derivative signal and P is the derivative peak-to-peak height. The $Ni(OMTBP)I_{2.9}$ crystals were too small for single crystal intensity measurements, so the EPR signal from a powdered sample was electronically integrated to yield an absorption curve. The area under the absorption curve was then integrated by the cut and weigh technique. Absolute EPR intensity measurements were made at room temperature by comparing the integrated absorption of the sample with that of a known amount of DPPH dispersed in KBr.

Electrical Conductivity Measurements. Electrical conductivity was measured at 27 Hz on single crystals by a four-probe ac phase-locked technique.[11] Electrical contacts between a given crystal and four 0.13-mm Al wires were made with a conductive paint prepared from palladium dust (0.25-0.55 μm) and a resin obtained from "Copper Print" (GC Electronics, Rockford, Ill.) by removing the powdered copper. Approximately five volumes of octyl acetate were added per volume of resin to achieve the desired drying rate and flow characteristics. A controlled ac current was driven through the crystal needle axis via contacts at the two ends of the crystal with the conductive paint "capping" the ends. Two additional contacts, symmetrically disposed between terminal current contacts, were made by applying a narrow, circular band of palladium paint around the needle axis of the crystal. The ac voltage developed between these inner contacts was processed by a PAR Model 128A lock-in amplifier, yielding a dc voltage proportional to the sample resistance. The sampling currents employed generally ranged from 1.0 to 10.0 μA, although the ohmic behavior of the materials was verified with currents ranging from 0.1 μA to 1.0 mA. Contact integrity was verified by the lead interchange technique.[12]

The temperature dependence of the electrical conductivity was determined by placing the sample crystal, appropriately shielded from gas currents, in a Dewar flask. Boil-off gas from a liquid N_2 or He reservoir was channeled through the Dewar and over the crystal holder. The crystal temperature was measured by a Cu-constantan thermocouple positioned within 3 mm of the enclosed crystal. The sample temperature was varied by controlling the cryogenic gas boil-off; cooling and warming rates were maintained in the vicinity of 0.8-2 °C/min.

The conductivity of the materials was calculated from the relationship $\sigma = L/RA$, where σ is the conductivity in $(\text{ohm cm})^{-1}$, R is the measured resistance (in ohms) of the material between the two inner contacts, L is the separation between the two inner contacts in cm, and A is the cross-sectional area of the sample in cm^2. The $Ni(OMTBP)I_{1.08}$ crystals are typically 0.09 cm long and are of octagonal cross section with octagonal faces being ~0.002 cm in width. The $Ni(OMTBP)I_{2.9}$ crystals are generally 0.1 cm long by 0.001 cm. Estimated uncertainty in these measurements is 2.0×10^{-4} cm. Because of the small crystal size, the area A could only be estimated from the maximum cross-sectional distance as observed with a microscope. An empirical analysis of measurement errors indicates that the area is uncertain by $\delta A/A \approx \pm 0.2$, leading to an uncertainty, $\Delta\sigma/\sigma \sim \pm 0.2$.

X-ray Study of $Ni(OMTBP)I_{1.08}$. On the basis of Weissenberg and precession photography, crystals of $Ni(OMTBP)I_{1.08}$ were assigned to Laue group $4/mmm$ of the tetragonal system. Systematic absences were observed for $hk0$, $h + k \neq 2n$; $0kl$, $l \neq 2n$. These absences are consistent with space group D_{4h}^{11}-$P4_2/nbc$. The cell constants of a = 21.011 (9) and c = 7.556 (5) Å were obtained by least-squares refinement[13,14] using the setting angles obtained by hand-centering 11 reflections on a FACS-I diffractometer employing Ni prefiltered Cu $K\alpha_1$ radiation.

In addition to the expected Bragg scattering, several diffuse layers were observed on the initial oscillation photographs. Diffuse scattering similar to that seen here has been observed in these laboratories[2d,15,16] and elsewhere[5,17,18] for several related systems and has been attributed to disorder of the iodine chain. In the present case, stationary crystal photographs indicate that the diffuse scattering is localized in planes normal to the tetragonal c axis. For the most part the diffuse layers in $Ni(OMTBP)I_{1.08}$ can be indexed on a superstructure spacing, c_d, of 19.46 Å. Since c_d is not a multiple of c, the Bragg repeat spacing, the superlattice is incommensurate with the Bragg lattice. An incommensurate superlattice was also found in $TTT_2(I_3)$.[6,18] However, there the superperiod of 9.46 Å was approximately equal to that found in several other well-characterized systems[5,16,17] in which the iodine-containing species was determined to be the triiodide ion. In the present case, c_d is about twice that reported for other systems. On this basis, it would be tempting to propose a supercell containing two triiodide ions. However, extensive measurement of the diffuse scattering by counter techniques reveals that the profiles of the diffuse sheets are not independent of order, and that the superlattice spacing c_d accounts only approximately for their positions. Similarly complex diffuse scattering has been interpreted for Hollandite[19] as arising from short-range order among atoms in a given channel. Indeed, broadening and shifting of the diffuse layers are expected in general[20] for chains not displaying long-range order. At present, we have found no totally satisfactory interpretation for the diffuse scattering in $Ni(OMTBP)I_{1.08}$ and here we limit discussion to our interpretation of the Bragg scattering.

Intensity data for the Bragg scattering were collected and processed in the usual manner,[13] using the θ-2θ scan technique. Of the total of 1591 unique reflections gathered 687 were found to have $F_o^2 \geq 3\sigma(F_o^2)$. Further experimental details and other crystal data are given in Table I.

An origin removed sharpened Patterson map indicated the positions of all nonhydrogen atoms relative to the nickel atom. With four formula units in the cell, the possible special positions for the nickel atom in $P4_2/nbc$ have symmetries $222(D_2)$ and $\bar{4}(S_4)$. Considering the orientation and conformation obtained from the Patterson map the

Table I. Crystal Data, Data Collection, and Refinement of $Ni(OMTBP)I_{1.08}$

compd	$Ni(OMTBP)I_{1.08}$
formula	$C_{44}H_{36}I_{1.08}N_4Ni$
formula wt	816.58 amu
cell a	21.011(9) Å
c	7.556(5) Å
V	3335.5 Å^3
Z	4
space group	D_{4h}^{11}-$P4_2/nbc$
crystal shape	needle of octagonal cross section bounded by faces of the forms {100}, {110}, and {001} with separations of 0.05, 0.04, 0.05, 0.05, and 0.251 respectively
radiation	Cu Kα(λ(Cu Kα_1) = 1.540 562 Å)
linear absorption coefficient	90.6 cm^{-1}
transmission coefficients	0.29-0.51
take-off angle	3.5°
receiving counter	34 cm from crystal
receiving aperture	6.8 mm high by 5.8 mm wide, 22.5 cm from crystal
scan speed	2.0°/min
scan width	1.0° above Kα_2 to 1.0° below Kα_1
background counts	40 s total for singly scanned peaks
data collected	$h \geq k \geq 0, \pm l, 2\theta \leq 125°$
unique data	1591
unique data with $\lvert F_o\rvert \geq 3\sigma(F_o^2)$	687
R for last cycle of refinement	0.050
R_w	0.056

only possible choice is the $\bar{4}$ site. Thus, the entire Ni(OMTBP) complex is constrained to have $\bar{4}$ symmetry; the asymmetric unit consists of one-quarter of the metal complex and one-quarter of an iodine atom. Several high peaks in the sharpened Patterson map at ($\frac{1}{2}$, 0, w) could be interpreted as nickel-iodine vectors; however, these peaks were rather poorly resolved in w. Initial least-squares refinements were based on the unique portion of the metal complex (except for hydrogen atoms) and two partially occupied positions for the disordered iodine atom. All such refinements resulted in high R indices (~0.95), and large thermal parameters for the iodine atoms. Two cycles of least-squares refinement using only data for which $l = 0, l \neq 2n, h + k \neq 2n$ (the z coordinates are irrelevant for $l = 0$ reflections and neither Ni nor I contributes to the l or $h + k \neq 2n$ reflections) resulted in agreement indices of 0.086 and 0.112, demonstrating that the light-atom model was essentially correct. At this point an ordinary Patterson map was examined with special attention to the line ($\frac{1}{2}$, 0, w). If the nickel atom is ordered, then this line is essentially the electron distribution function of the disordered iodine atom. The vector density along this line consists of one very broad peak which reaches a maximum at $w = \frac{1}{4}$ and a minimum at $w = 0$ (and $w = \frac{1}{2}$). The maximum-to-minimum vector density ratio is approximately 2.0. As a starting point, then, it seemed a better approximation to ignore the presence of iodine altogether (except for $l = 0$ reflections) rather than to attempt refining partially occupied positions. A structure factor calculation with no iodine contribution for reflections with $l \neq 0$ yielded agreement indices of 0.14 and 0.22. The main feature of the subsequent Fourier map was a very broad peak of 28.1 e/Å^3 centered at $\frac{1}{4}$, $\frac{1}{4}$, 0, which tailed off to a value of 12.3 e/Å^3 at $\frac{1}{4}$, $\frac{1}{4}$, $\frac{1}{4}$. Owing to the severity of this disorder, modeling the observed electron density distribution by refinement of occupancy and thermal parameters of several partially occupied positions along the line $\frac{1}{4}$, $\frac{1}{4}$, z is ineffective. As an alternative to this approach, we have treated the disordered iodine atom as a statistical distribution of electron density in much the same way as thermal motion is ordinarily taken into account. For thermal motion the functional form is that of a Gaussian distribution[21] of electron density centered at the atomic position. However, when dealing with a disordered system some distribution other than a Gaussian may yield a better approximation to the observed distribution, thus allowing further refinement of the remainder of the structure and better agreement with experiment. The main practical advantages of this approach are that very few independent parameters are needed (typically one or two), the total occupancy of the disordered atom can be readily obtained (mainly from the $l = 0$ reflections), and problems of oscillation and correlation arising from the least-squares refinement of many similar partially occupied positions (see ref 18, for example) are eliminated. The principal disadvantage of this method is that finding a suitable distribution is largely a matter of trial and error. For $Ni(OMTBP)I_{1.08}$ we have tried several distribution functions, and find that the following cosine function gives quite acceptable agreement with experiment (Figure 1). Let $p(z)$ be the normalized probability of finding an iodine atom between z and $z + dz$. Then the form adopted here is $p(z) = \Omega(\pi^{-1} + 0.5w)^{-1}(\cos 2\pi z + w)$, where Ω and w are variable parameters to be determined from the data. The variable Ω is related to the number of iodine atoms per unit cell while w determines the shape of the distribution. Once the cosine distribution was chosen, the remainder of the refinement proceeded in the usual fashion. All hydrogen atoms were located in a single difference Fourier map; their positions were then adjusted to idealize geometry and they were not refined in the least-squares process. In the final cycle of anisotropic refinement there were 114 variables (including two for the cosine distribution) and 687 data; the final values of R and R_w are 0.050 and 0.056, respectively. The ratio of I to Ni(OMTBP), as determined in this refinement, is 1.08 (1).

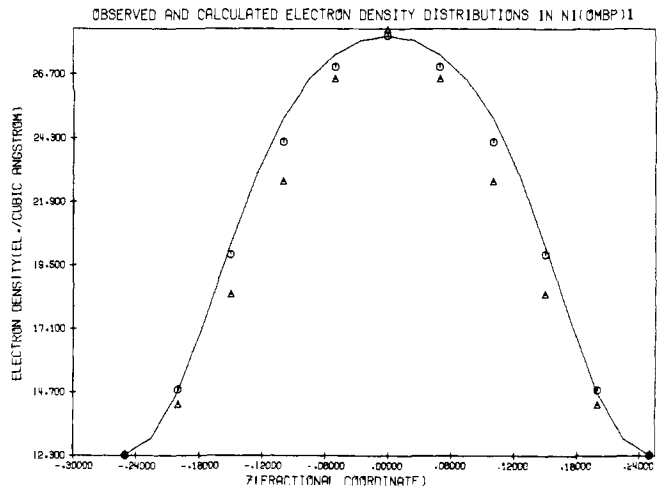

Figure 1. A plot of observed (—) vs. calculated electron density along the line $\frac{1}{4}$, $\frac{1}{4}$, z: △, calculated for a triangular distribution of electron density; ○, calculated for a cosine distribution of electron density.

Except for one peak of 1.31 e/Å^3 midway between the nickel atoms, the final difference Fourier map is featureless. Examination of $\Sigma w(\lvert F_o\rvert - \lvert F_c\rvert)^2$ as a function of $\lambda^{-1}\sin\theta$, setting angles, and Miller indices revealed no unusual trends. Specifically, agreement for the l-even reflections is as good as or better than that for the l-odd reflections, indicating that refinement of the statistical model for the disordered iodine atom was successful. The final positional and thermal parameters are given in Table II, and root-mean-square amplitudes of vibration in Table III.[22] A listing of structure amplitudes is available.[22]

Results

Resonance Raman Spectra. Determination of the stoichiometric formulas $Ni(OMTBP)I_{1.08}$ and $Ni(OMTBP)I_{2.9}$ by chemical analysis gives no information about the charge on the macrocyclic complex, since iodine can assume a variety of forms (I_2, I^-, I_3^-, I_5^-, etc.) in the crystal. Moreover, the Bragg scattering, while providing the Ni:I ratio in $Ni(OMTBP)_{1.08}$, yields no information in the present instance about species present, save that iodine atoms are severely disordered. In order to relate the transport properties of $Ni(OMTBP)I_{1.08}$ and $Ni(OMTBP)I_{2.9}$ to the degree of oxidation by I_2 of the macrocycle and thus to "band filling", the state of the iodine must be determined. Resonance Raman spectroscopy is particularly useful for this task.[4] The resonance Raman spectra of $Ni(OMTBP)I_{1.08}$ and $Ni(OMTBP)I_{2.9}$ are shown in Figure 2. The two spectra are virtually identical. The sharp absorption at 107 cm^{-1} and the higher order overtone progression are characteristic[4] of the polyiodide species, I_3^-. Neither I_2 nor

Table II. Positional and Thermal Parameters for the Atoms of Ni(OMTBP)$I_{1.08}$

atom	x^a	y	z	$\beta_{11}{}^b$ or B, Å^2	β_{22}	β_{33}	β_{12}	β_{13}	β_{23}
Ni	−¼	¼	−¼	13.02(29)	13.02	164.6(50)	0	0	0
N(1)	−0.158 58(22)	0.266 57(20)	−0.243 01(87)	13.6(11)	12.4(13)	138.(13)	−0.14(82)	1.0(39)	−1.0(42)
C(1)	−0.129 97(32)	0.322 88(33)	−0.191 59(92)	15.4(16)	14.4(17)	112.(19)	−2.8(13)	4.9(41)	−0.7(41)
C(2)	−0.060 44(30)	0.315 57(31)	−0.188 67(91)	14.2(17)	17.0(18)	159.(20)	−1.5(12)	−4.1(40)	15.0(42)
C(3)	−0.011 44(31)	0.356 56(34)	−0.136 17(96)	14.7(20)	20.9(20)	176.(19)	−3.3(14)	−1.0(47)	6.2(51)
C(4)	0.049 84(35)	0.333 33(37)	−0.1537(11)	16.8(19)	25.2(22)	198.(21)	−7.5(18)	−3.6(51)	9.4(53)
C(5)	0.062 82(30)	0.273 17(38)	−0.2232(11)	11.2(15)	35.2(24)	190.(22)	0.6(14)	−3.7(46)	18.2(60)
C(6)	0.014 86(30)	0.231 72(32)	−0.2757(10)	13.2(15)	22.2(21)	162.(21)	1.2(12)	3.5(47)	7.2(51)
C(7)	−0.048 48(25)	0.254 45(32)	−0.2555(11)	14.4(13)	17.4(14)	153.(15)	−1.9(16)	−1.9(62)	5.9(52)
C(8)	−0.110 33(29)	0.224 43(30)	−0.284 83(90)	14.5(16)	17.0(15)	122.(18)	0.6(12)	5.2(40)	4.5(41)
C(9)	−0.161 64(33)	0.379 54(34)	−0.170 57(97)	15.0(18)	14.5(19)	171.(19)	−5.5(14)	0.6(44)	−9.8(45)
C(10)	−0.020 71(35)	0.422 60(36)	−0.0624(10)	19.5(19)	24.8(22)	219.(23)	−3.6(17)	−20.3(48)	0.7(48)
C(11)	0.032 38(33)	0.166 67(38)	−0.3491(11)	14.8(19)	26.5(23)	233.(20)	2.6(16)	8.7(49)	16.5(55)
HlC(4)	0.084	0.359	−0.114	4.9					
HlC(5)	0.106	0.260	−0.235	5.0					
HlC(9)	−0.139	0.414	−0.118	4.0					
HlC(10)	0.020	0.440	−0.029	5.1					
H2C(10)	−0.039	0.449	−0.152	5.1					
H3C(10)	−0.048	0.421	0.036	5.1					
HlC(11)	0.020	0.135	−0.266	5.0					
H2C(11)	0.011	0.160	−0.458	5.0					
H3C(11)	0.077	0.165	−0.365	5.0					

[a] Estimated standard deviations in the least significant figure(s) are given in parentheses in this and all subsequent tables. [b] The form of the anisotropic thermal ellipsoid is $\exp[-(\beta_{11}h^2 + \beta_{22}k^2 + \beta_{33}l^2 + 2\beta_{12}hk + 2\beta_{13}hl + 2\beta_{23}kl)]$. The quantities given in the table are the thermal coefficients $\times 10^4$.

I_5^- is present (≤2%), as indicated by the absence of their sharp fingerprint absorptions at 212 and 167 cm^{-1}, respectively. ^{129}I-Mössbauer spectroscopic examination of a related material, Ni(Pc)I_x,[2a,6] indicates a complete absence of I^- over a range of stoichiometries. By analogy we assume that this is also true for the present compounds. Thus, a reasonable formulation of Ni(OMTBP)I_x is Ni(OMTBP)$(I_3)_\rho$, where $\rho = x/3$ is the actual degree of partial oxidation of the macrocycle.

Description of the Structure of Ni(OMTBP)$(I_3)_{0.36}$. This structure consists of stacks of Ni(OMTBP) ions segregated from chains of iodine which run parallel to the c axis. A stereoview of the crystal packing is shown in Figure 3. The atomic labeling scheme and a perspective view of the molecule are given in Figure 4; bond lengths and angles are provided in Table IV. The Ni(OMTBP) ion has imposed symmetry $\bar{4}$. The Ni-Ni separation of 3.778 (5) Å along the chain is about 0.50 Å longer than that found in Ni(dpg)$_2$I,[15] Ni(bqd)$_2$I$_{0.5}$,[15] or Ni(Pc)I.[2d,6] The iodide chains are located in channels formed by the benzo groups of adjacent Ni(OMTBP) ions. Although the precise state of order of the iodine chain is not known, several qualitative statements can be made on the basis of the X-ray scattering measurements. The derived occupancy factor for the disordered iodine atom yields a value of 1.08 (1) iodine atoms per Ni(OMTBP) complex in the crystal. This value would be 1.16 if the iodine chain were completely ordered with an incommensurate repeat of 19.46 Å, and if there were six iodine atoms per supercell. The diffuse scattering measurements suggest that each chain individually is disordered to some extent. The statistical refinement indicates that this disorder results in fewer iodine atoms per channel than would be expected on the basis of a simple incommensurate model, and also results in a pronounced preference for the site at (¼, ¼, 0) relative to the site at (¼, ¼, ¼). Such a preference could be explained in terms of a constriction of the channel at (¼, ¼, ¼), since there are several channel-to-hydrogen-atom contacts of 3.03 Å at this point, whereas the closest such contact at (¼, ¼, 0) is 3.51 Å (Figure 3).

To the best of our knowledge this is the first report of benzporphyrin structure. There is, however, a large body of literature available for other porphyrins,[23] and for the closely related phthalocyanine molecule (ref 2d and references cited therein). The present complex is similar, where comparisons are possible, to the closely related M(TPP)[6] and M(OEP)[6] complexes. Thus, with the possible exception of the C_a-C_b and M···C_m separations, the values in Table IV are well within the range previously reported for metalloporphyrins. The bond lengths in the fused benzene ring range from 1.383 (9) to 1.422 (9) Å; their mean is normal at 1.399 (9) Å. The angles within the benzene ring fall into two classes, C(2)-C(3)-C(4) and C(5)-C(6)-C(7) forming one class with a mean of 116.0 (1)°, the other four angles being equivalent with a mean of 122.0 (5)°. A similar pattern can be found in all phthalocyanine structures (see ref 2d and references cited therein), the result being attributed to strain caused by fusion of the five-membered ring. The mean plane of the molecule as a whole is constrained by symmetry to be $z = -¼$. However, the molecule is markedly nonplanar, with deviations from the mean plane ranging up to 1.42 Å. Best weighted least-squares planes are given in Table V. The isoindole moieties are essentially planar, with the average deviation of an atom from the plane being 0.026 Å; the methyl carbon atoms do not deviate significantly from this plane while the Ni atom does at 0.11 Å. Owing to the $\bar{4}$ symmetry, the distortion of the essentially square-planar coordination is a tetrahedral one. Adjacent isoindole rings are tilted at an angle of about 40° to each other and 20° to the plane $z = -¼$. The net result of these large tilts from the mean plane is a saddle-shaped molecule, where we take adjacent pairs of methyl groups to be alternatively the peaks and troughs of the saddle. The reason for the unusually large distortions from planarity exhibited by this molecule is probably the accommodation of the bulky methyl substituents. Adjacent methyl groups are bent away from each other via an opening of the C(2)-C(3)-C(10) and C(7)-C(6)-C(11) angles from 120° to about 125°. The closest intermolecular approach of two nonhydrogen atoms is 3.46 Å between atom C(6) and one of its symmetry equivalents one molecule down in the stack.

Magnetic Properties. Single crystals of Ni(OMTBP)$(I_3)_{0.36}$ and Ni(OMTBP)$(I_3)_{0.97}$ exhibit a single, rather narrow EPR signal whose g value and line width are dependent on the crystal orientation in the external field. The detailed study of this signal serves to identify the nature of the orbital which loses an electron upon partial oxidation of the macrocycle, yields information about the intermolecular interaction within the

Table IV. Intramolecular Bond Distances and Angles in Ni(OMTBP)$I_{1.08}$

atoms	type[a]	distance, Å
Ni-N(1)	M-N	1.953(5)
N(1)-C(1)	N-C_a	1.383(7)
N(1)-C(8)	N-C_a	1.383(7)
C(1)-C(2)	C_a-C_b	1.469(9)
C(1)-C(9)	C_a-C_m	1.373(9)
C(2)-C(3)		1.400(9)
C(2)-C(7)	C_b-C_b	1.403(9)
C(3)-C(4)		1.383(9)
C(3)-C(10)		1.508(9)
C(4)-C(5)		1.396(9)
C(5)-C(6)		1.390(9)
C(6)-C(7)		1.422(8)
C(6)-C(11)		1.520(9)
C(7)-C(8)	C_a-C_b	1.461(8)
C(8)-C(9′)	C_a-C_m	1.378(9)
Ni···C(9)	M···C_m	3.349(7)
Ni···C(8)	M···C_a	2.995(6)
Ni···C(1)	M···C_a	2.983(6)
atoms	**type**	**angle, deg**
N(1)-Ni-N(1)′	NMN	90.94(1)
N(1)-Ni-N(1)″	NMN	176.9(4)
Ni-N(1)-C(1)	MNC_a	126.0(4)
Ni-N(1)-C(8)	MNC_a	126.9(4)
C(1)-N(1)-C(8)	C_aNC_a	107.1(5)
C(2)-C(1)-C(9)	$C_bC_aC_m$	124.8(6)
N(1)-C(1)-C(2)	NC_aC_b	110.3(6)
N(1)-C(1)-C(9)	NC_aC_m	124.3(6)
C(1)-C(2)-C(7)	$C_aC_bC_b$	105.6(5)
C(1)-C(2)-C(3)		132.2(7)
C(3)-C(2)-C(7)		122.2(6)
C(2)-C(3)-C(10)		125.2(6)
C(2)-C(3)-C(4)		116.1(7)
C(4)-C(3)-C(10)		118.7(7)
C(3)-C(4)-C(5)		122.5(6)
C(4)-C(5)-C(6)		122.2(6)
C(5)-C(6)-C(7)		115.9(6)
C(5)-C(6)-C(11)		119.5(6)
C(7)-C(6)-C(11)		124.6(6)
C(2)-C(7)-C(6)		120.9(6)
C(6)-C(7)-C(8)		132.1(6)
C(2)-C(7)-C(8)	$C_aC_bC_b$	106.9(5)
N(1)-C(8)-C(7)	NC_aC_b	109.9(5)
N(1)-C(8)-C(9′)	NC_aC_m	123.8(6)
C(7)-C(8)-C(9′)	$C_bC_aC_m$	125.0(6)
C(1)-C(9)-C(8′)	$C_aC_mC_a$	124.7(7)

[a] The notation is that of Hoard, J. L. *Science* **1971**, *174*, 1295-1302.

$Ni(OMTBP)^{\rho+}$ stack, and gives substantial information about the crystal structure of the $\rho = 0.97$ material.

a. *g*-Values. The single crystal EPR spectra of $Ni(OMTBP)(I_3)_{0.36}$ and $Ni(OMTBP)(I_3)_{0.97}$ consist of a single Lorentzian line in all orientations. For $Ni(OMTBP)(I_3)_{0.36}$ this is entirely consistent with the crystal structure. The g tensor for both crystals is axially symmetric with the needle (c) axis corresponding to the unique ($\|$) tensor axis. The angle-dependent g value for the two materials, $g(\theta)$, can be written $g(\theta) = [g_\|^2 \cos^2\theta + g_\perp^2 \sin^2\theta]^{1/2}$, where θ is the angle between the magnetic field, H_0, and c. A least-squares fit to the equation gives $g_\| = 2.0102$ (2) and $g_\perp = 2.0033$ (2) for $Ni(OMTBP)(I_3)_{0.36}$ and $g_\| = 2.0108$ (4) and $g_\perp = 2.0029$ (4) for $Ni(OMTBP)(I_3)_{0.97}$. The observed angle dependence and appreciable intensity of the signal indicate that for both materials the signal truly represents the paramagnetic resonance of a hole species produced by iodine oxidation rather than an impurity.

In both materials $g_\|$ and $g_\perp$ are very close to the free-electron value of $g_e = 2.0023$. A metal-centered oxidation, however, would yield a hole species with the g values of $[Ni^{III}(OMTBP)]^+$ far from g_e. For example, the values are $g_\perp = 2.29$ and $g_\| = 2.11$ for the closely related $[Ni^{III}Pc]^+$ cation.[24] The combination of nearly free electron g values and narrow line widths is instead what is expected of the octamethyltetrabenzporphyrin π cation radical, $[Ni^{II}(OMTBP)]^+$; thus the oxidation is ligand centered.

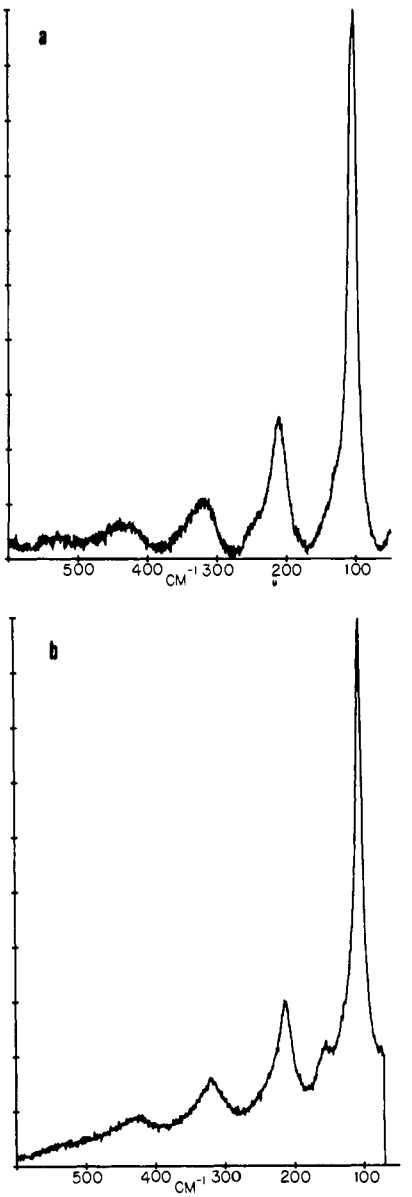

Figure 2. Resonance Raman spectra of (a) $Ni(OMTBP)(I_3)_{0.36}$ and (b) $Ni(OMTBP)(I_3)_{0.97}$ with 5145-Å excitation source. The ordinate scale is in relative photomultiplier counts/s.

A closer inspection of the g tensor, nevertheless, shows it to be anomalous. For either a π cation radical or for a planar Ni^{III} species one expects $g_\perp > g_\| \approx g_e$. However, for $Ni(OMTBP)(I_3)_{0.36}$ and $Ni(OMTBP)(I_3)_{0.97}$, as well as for the related material Ni(Pc)I,[2d] $g_\| > g_\perp \sim g_e$. We now show that the observed g values are precisely of the form expected if a very small fraction of the hole density resides on the iodine chain.

If we consider a partially oxidized metallomacrocycle, $(ML)^{\rho+}(I_3^-)_\rho$, then, in the absence of any electronic interaction between the $[(ML)^{\rho+}]_n$ stack and I_3^- chain, the wave function for a crystal might be written schematically as $|[(ML)_{\rho-1}]^+(I_3^-)\rangle$. The simplest way to account for spin density on iodine involves the inclusion of a small degree of back charge transfer from I_3^- to the macrocyclic stack. We

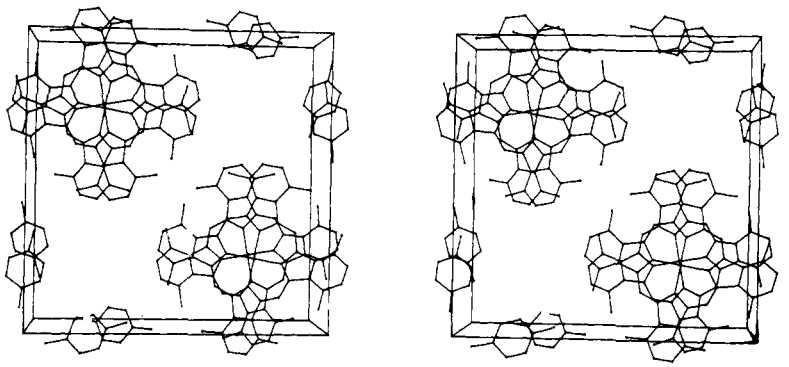

Figure 3. Stereoview of the unit cell of $Ni(OMTBP)(I_3)_{0.36}$. Hydrogen atoms have been omitted.

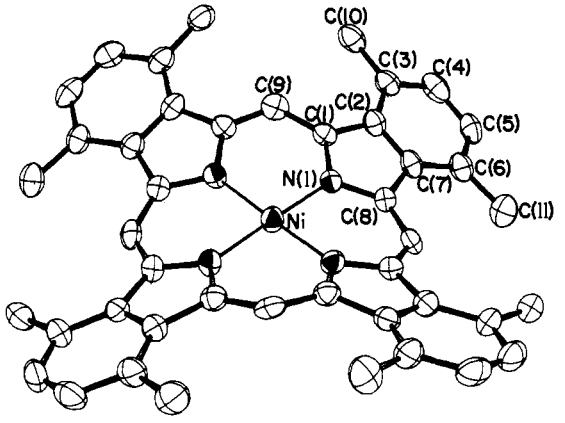

Figure 4. A perspective drawing of the Ni(OMTBP) molecule, showing the labeling scheme. Hydrogen atoms have been omitted.

write a simple Mulliken charge transfer wave function

$$|\psi\rangle = (1 - \alpha^2)^{1/2}|(Ni(OMTBP))_{\rho^{-1}}{}^{+}(I_3^-)\rangle + \alpha|(Ni(OMTBP))_{\rho^{-1}}(I_3^{\cdot})\rangle$$

in which α^2 represents the degree of charge transferred from I_3^- back to the partially oxidized macrocycle. If we assume a ligand-centered oxidation of Ni(OMTBP), a small but nonzero α^2 can account for the observed g tensor. This analysis also provides a further argument against a metal-centered oxidation. In this model, the g values for $Ni(OMTBP)(I_3)_\rho$ are given by

$$g_i = (1 - \alpha^2)g_i(Ni(OMTBP))^+ + \alpha^2 g_i(I_3^{\cdot})$$

where $g_i = g_\parallel$ or $g_\perp$ and reference g values for the isolated component species are to be used. A linear ($I_3^{\cdot}$) free radical would have three electrons residing in a doubly degenerate π^* orbital pair, split into two Kramers doublets by spin-orbit coupling. For such a species one obtains in first order[25]

$$g_\parallel = g_e + 2l[\lambda^2/(\lambda^2 + \Delta^2)]^{1/2}\, g_\perp = g_e[\Delta^2/(\lambda^2 + \Delta^2)]^{1/2}$$

where λ is the iodine spin-orbital coupling constant, l represents a correction to the angular momentum about the symmetry axis, and Δ represents any "crystal field" splitting of the π^* orbital. A finite value of α^2 will give a positive contribution to $g_\parallel$ and a slightly decreased $g_\perp$, thereby leading to $g_\parallel > g_\perp$, as is observed. For the I_3^- in $Ni(OMTBP)(I_3)_{0.36}$, Δ must be zero because of the fourfold symmetry at I. Therefore, neglecting deviations of l from unity, reference g values for an axially symmetric $I_3^{\cdot}$ are $g_\perp(I_3^{\cdot}) = 0$ and $g_\parallel(I_3^{\cdot}) = g_e + 2 = 4$.

If the oxidation in $Ni(OMTBP)(I_3)_\rho$ is metal centered, the reference g values for the hypothetical $(Ni(OMTBP))_{\rho^{-1}}{}^{+}$ fragment would be expected to be $g_\perp \approx 2.29$ and $g_\parallel \approx 2.11$ as is found for $(Ni^{III}Pc)^+$.[24] No consistent fit of our experimental results is possible if such reference g values are employed. This confirms the qualitative argument for the oxidation being ligand centered. However, if we take the oxidation to be ligand centered, then the reference g values should be those of the cation radical ($Ni^{II}(OMTBP)^+$), which are expected to be $g_\perp \geq g_\parallel \approx g_e$. Within the accuracy of these considerations it is sufficient to take $g_\perp \sim g_\parallel \sim g_e$, since the g tensor for the related compound ($Ni^{II}Pc^+$) is roughly isotropic and close to the free-electron value (2.0023).[24] We thus arrive at the equation for $g_\parallel$ in $(ML)(I_3)_\rho$

$$g_\parallel = g_e + 2\alpha^2$$

From the measured g values, the degree of back charge transfer from an I_3^- ion to the macrocyclic stack in both $Ni(OMTBP)(I_3)_{0.36}$ and $Ni(OMTBP)(I_3)_{0.97}$ is $\alpha^2 = 0.004$.

The g anisotropy in the two $Ni(OMTBP)(I_3)$ crystals is determined by the small spin density on I_3^-, and thus $g_\parallel$, which lies along the needle axis in both crystals, must coincide with the triiodide internuclear axis. This is confirmed by the X-ray structure of the $\rho = 0.36$ crystals. We therefore conclude that the I_3^- ions in $Ni(OMTBP)(I_3)_{0.97}$ are also aligned parallel to the needle axis.

b. Line Width of $Ni(OMTBP)(I_3)_{0.36}$. The exchange-narrowed EPR line of $Ni(OMTBP)(I_3)_{0.36}$ is Lorentzian at room temperature for all orientations, and remains so down to ~40 K. As the temperature is lowered further, the signal begins to exhibit some asymmetry. The temperature at which this asymmetry becomes apparent is dependent on the orientation of the crystal in the magnetic field. With $H_0 \perp c$, the line is Lorentzian down to 40 K; below this temperature the high-field side of the line begins to broaden. With $H_0 \parallel c$, similar behavior becomes evident only at 20 K. As shown below, the conductivity in this temperature regime is far too low for this asymmetry to arise from a Dysonian[26] contribution to the width.

At room temperature the peak-to-peak derivative linewidth, Γ, is an axially symmetric function of the field orientation, with the unique direction along the needle axis, c. The angle dependence (Figure 5) can be fit to the equation

$$\Gamma(\theta) = \Gamma_0 + \Gamma_1(1 + \cos^2\theta) \qquad (1)$$

where $\Gamma_0 = 3.51$ G and $\Gamma_1 = 1.72$ G. This functional form is similar to that of an exchange-narrowed line in which the broadening interaction is the intermolecular electron-electron dipolar interaction between spins on the Ni(OMTBP) chain.[27-29]

As the temperature is lowered from 300 K to approximately 140 K, the line width retains the angular dependence of eq 1, but decreases exponentially with an apparent activation energy of $\Delta \sim 0.035$ (5) eV (Figure 6). Below 140 K the line width changes less rapidly, eventually becoming T independent. The quantity $\Gamma(\theta)$ also begins to deviate from the form of eq 1. For example, for 25 K $\lesssim T \lesssim$ 60 K, $\Gamma(0) = \Gamma(90°)$ and there is a

Table V. Least-Squares Planes in Ni(OMTBP)$I_{1.08}$

atoms	deviations from plane, Å				
	plane 1[a]	plane 2	plane 3	plane 4	plane 5
Ni	0	−0.110	−0.245	−0.246	−0.282
N(1)	−0.053	−0.015(6)[b]			−0.109(6)
C(1)	−0.441	0.026(7)			−0.020(7)
C(2)	−0.463	−0.026(7)	0.004(6)	0.002(6)	−0.020(7)
C(3)	−0.860		0.004(7)	0.002(7)	−0.031(7)
C(4)	−0.728		−0.010(8)	−0.012(8)	−0.015(8)
C(5)	−0.203		0.006(8)	0.004(8)	0.042(8)
C(6)	0.194		0.003(8)	0.001(8)	0.051(8)
C(7)	0.041	0.002(8)	−0.008(8)		0.009(8)
C(8)	0.263	0.001(7)			−0.075(7)
C(9)	−0.600				0.219(7)
C(10)	−1.418			0.007(8)	−0.069(8)
C(11)	0.749			0.008(8)	
C(9′)	0.600				
std dev		0.0176	0.006	0.006	0.064

Plane Equations: $Ax + By + Cz = D$

plane no.	*A*	*B*	*C*	*D*
1	0.0	0.0	−7.556	1.889
2	0.301	7.071	−7.114	3.581
3	0.809	7.983	−6.983	3.784
4	0.804	7.985	−6.983	3.787
5	1.087	7.457	−7.053	3.638

Interplanar Angles (deg)

plane no.	plane no.	angle	plane no.	plane no.	angle
1	2	19.69	2	4	3.01
1	3	22.46	2	5	2.43
1	4	22.46	3	4	0.01
1	5	21.02	3	5	1.71
2	3	3.02	4	5	1.72

[a] Plane 1 is the plane $z = -1/4$. [b] Standard deviations are given for those atoms used in the definition of a particular plane.

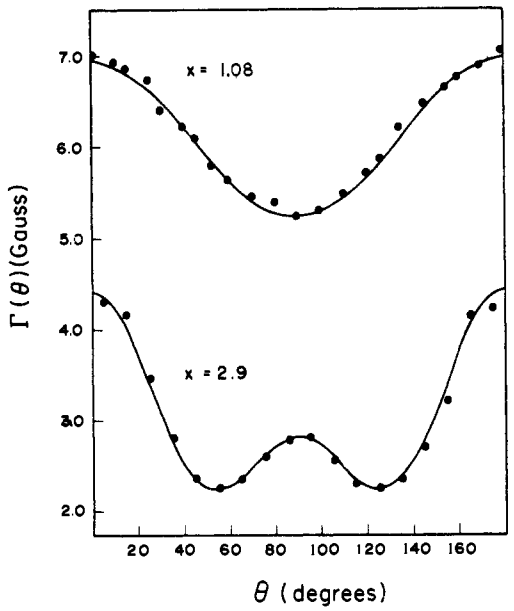

Figure 5. Angular dependence of EPR-determined line widths at ambient temperature for Ni(OMTBP)$(I_3)_{0.36}$ (top) and Ni(OMTBP)$(I_3)_{0.97}$ (bottom). Solid lines are theoretical fits to eq 1 (top) and 2 (bottom).

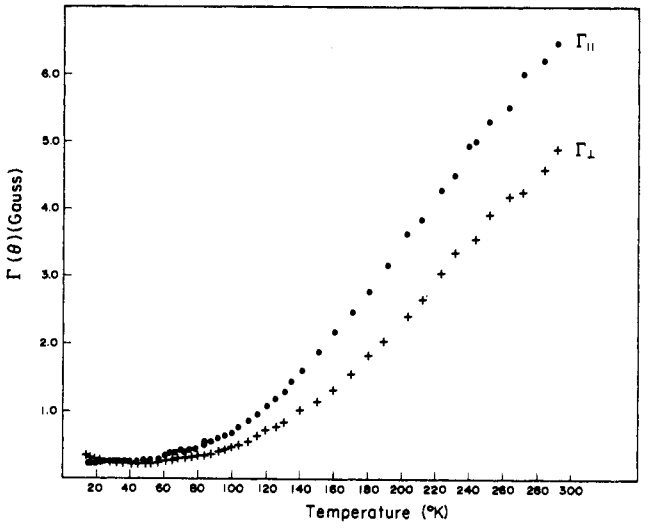

Figure 6. Temperature dependence of line width for a Ni(OMTBP)$(I_3)_{0.36}$ crystal oriented with [001] along the static field (●) and with [001] oriented ⊥ to static field (+).

line-width minimum at an intermediate angle. Below ~25 K, the signal asymmetry also increases.

c. Line Width of Ni(OMTBP)$(I_3)_{0.97}$. The room temperature[30] single crystal EPR line of Ni(OMTBP)$(I_3)_{0.97}$ is also an exchange-narrowed Lorentzian for all orientations. The peak-to-peak derivative line width function $\Gamma(\theta)$ is axially symmetric and can be fit to the equation

$$\Gamma(\theta) = \Gamma_0 + \Gamma_1(3\cos^2\theta - 1)^2 \qquad (2)$$

where $\Gamma_0 = 2.26$ G and $\Gamma_1 = 0.54$ G (Figure 5). This angle dependence is similar to that seen for an electron spin dipole-dipole interaction which is exchange narrowed, but with $\omega_e < \omega_L$, in contrast to the result for Ni(OMTBP)$(I_3)_{0.36}$.[27] Note that for all orientations $\Gamma(\theta)$ for the $\rho = 0.97$ crystal is less than that for $\rho = 0.36$ material.

The observation of an axial line width and the coincidence of the unique direction of the line-width functions ($\theta = 0$) with

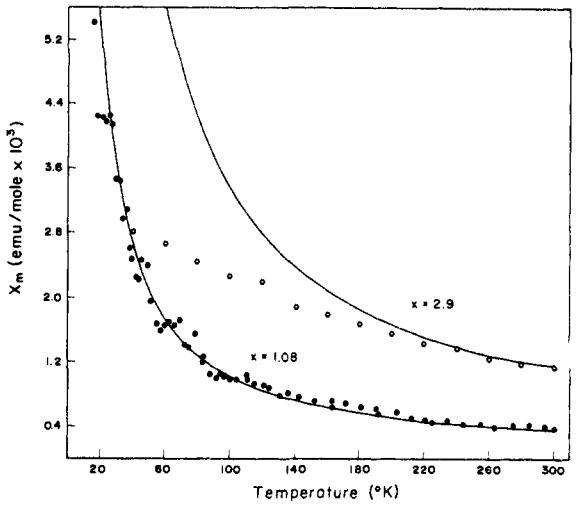

Figure 7. Temperature-dependent EPR intensity. The lower data set is for a single crystal of Ni(OMTBP)$(I_3)_{0.36}$ oriented with the field parallel to [001] and includes a least-squares fit of the data to a Curie-law function. The upper set is the EPR intensity for powdered Ni(OMTBP)$(I_3)_{0.97}$. The solid trace is a calculated, hypothetical Curie-law response scaled to the ambient temperature susceptibility.

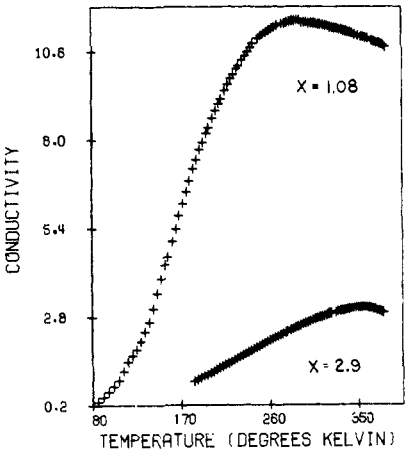

Figure 8. Four-probe electrical conductivity along the [001] axis as a function of temperature for Ni(OMTBP)$(I_3)_{0.36}$ (top) and Ni(OMTBP)$(I_3)_{0.97}$ (bottom). Sampling currents are nominally 1.0–10.0 μA root mean square.

the needle axis for $\rho = 0.97$ suggest that the Ni(OMTBP) moieties in these crystals also stack in columns along c.

d. Susceptibility. i. Ni(OMTBP)$(I_3)_{0.36}$. The static magnetic susceptibility, χ_m^s, of Ni(OMTBP)$(I_3)_{0.36}$ was measured between 400 and 100 K. The paramagnetic susceptibility, χ_ρ, was obtained by subtracting the temperature-independent diamagnetic contribution, χ_d^s, from χ_m^s. The value $\chi_d^s(I_3^-) = -4.7 \times 10^{-5}$ emu/mol was calculated from Pascal's constants for I_2 and I^-;[32] χ_d^s(Ni(OMTBP)) $= -4.13 \times 10^{-4}$ emu/mol for the parent compound was measured, and agrees well with the value calculated from Pascal's constants. The total diamagnetic susceptibility for Ni(OMTBP)$(I_3)_{0.36}$ is $\chi_d^s = -4.60 \times 10^{-4}$ emu/mol. The measured room temperature susceptibility, $\chi_m^s = -7.0 \times 10^{-5}$ emu/mol, then corresponds to a paramagnetic contribution $\chi_\rho = 3.9\ (9) \times 10^{-4}$ emu/mol, equivalent to 0.39 (8) spins ($S = \frac{1}{2}$, $g = 2$) per macrocycle. The absolute EPR intensity measurements give 0.40 (4) spins per macrocycle, in excellent agreement.

The susceptibility measurements were performed over the extended range 20–320 K by EPR methods, and Figure 7 plots the signal intensity, along with a calculated Curie-law curve. There are no detectable deviations from Curie behavior at or above 20 K.

These results may be used to place an upper bound on any exchange coupling between spins. If we first assume that the susceptibility (EPR intensity) obeys the singlet-triplet law

$$\chi_\rho = \frac{2Ng^2\mu\beta^2}{3kT}(1 + \exp(J/kT)/3) \qquad (3)$$

and further assume that at 20 K a 5% decrease in χ_ρ from the Curie value could have gone undetected, then applying eq 3 indicates that $J < 3$ cm^{-1}. Alternatively, if we assume that χ_ρ follows the Bonner-Fisher curve for an antiferromagnetically coupled one-dimensional Heisenberg chain of $S = \frac{1}{2}$ spins, then inspection of Figure 14, ref 32, or use of the equation in footnote 60, ref 33, leads to a similar conclusion about J.

ii. Ni(OMTBP)$(I_3)_{0.97}$. The static susceptibility of Ni(OMTBP)$(I_3)_{0.97}$, $\chi_m^s = 5.51 \times 10^{-4}$ emu/mol, was measured at room temperature by subtraction as described above. The diamagnetic contribution was also determined as described above giving $\chi_d^s = -5.49 \times 10^{-4}$ emu/mol. The resulting room temperature static paramagnetic susceptibility of Ni(OMTBP)$(I_3)_{0.97}$ is $\chi_\rho = 1.1\ (1) \times 10^{-3}$ emu/mol and corresponds to 0.90 (20) ($g = 2$, $S = \frac{1}{2}$) spins per molecule. Absolute EPR intensity measurements indicated 0.80 (6) ($g = 2$, $S = \frac{1}{2}$) in good agreement with the static measurements.

The EPR susceptibility as a function of temperature from 400 to 20 K is shown in Figure 7. In contrast to the results obtained for Ni(OMTBP)$(I_3)_{0.36}$, the susceptibility of Ni(OMTBP)$(I_3)_{0.97}$ does deviate from the Curie law. However, exchange coupling is small. Application of the Bonner-Fisher curve would require $J < 10$ cm^{-1}, since the susceptibility does not show a peak above ~20 K, but would peak in this model at the temperature $T_{max} = J/1.3k$.[32]

e. Conductivity. The temperature responses of the electrical conductivity along the needle axis ($\sigma_\parallel(T)$) for Ni(OMTBP)-$(I_3)_{0.36}$ and Ni(OMTBP)$(I_3)_{0.97}$ are shown in Figure 8. As the temperature is lowered from 380 K, the conductivity of Ni(OMTBP)$(I_3)_{0.36}$ is metal-like. It increases slowly, reaching a broad maximum $\sigma_\parallel^m$ centered at $T_m \sim 300$ K. The value of T_m is somewhat sample dependent, ranging from ~260 to 330 K, as is $\sigma_\parallel^m$, which ranges from 16 to 4 S cm^{-1}. The observed variations presumably reflect differences in crystal quality. Below T_m, down to the lower limit of the experiment of 45 K, the conductivity decreases in an activated manner. In this activated region, the value of $\Delta(T) = d(\ln \sigma)/d(1/T)$ increases slowly with decreasing temperature and by 160 K reaches a constant temperature value of $\Delta(0) \sim 0.045$ (6) eV.

The conductivity curve of Ni(OMTBP)$(I_3)_{0.97}$ (Figure 8) is qualitatively similar to that of Ni(OMTBP)$(I_3)_{0.36}$, with roughly a fourfold lower value of σ^m and a value $T_m \approx 340$ K, roughly 40–80 K higher than T_m for Ni(OMTBP)$(I_3)_{0.36}$. Again for the $\rho = 0.97$ crystal the conductivity maximum is sample dependent with T_m varying from 330 to ~380 K and $\sigma_\parallel^m$ ranging from 4.0 to 1.0 S cm^{-1}.[34] Below T_m the conductivity is activated with a constant activation energy $\Delta(0) \sim 0.050$ (6) eV below 220 K. Within experimental error this is the same activation energy as that exhibited by Ni(OMTBP)-$(I_3)_{0.36}$.

The form of the temperature dependence of σ for the two Ni(OMTBP)$(I_3)_\rho$ crystals is similar to that displayed by the tetracyanoplatinate, metal-based conductors, as well as by a number of moderately good organic conductors: as T increases from 0 K, $\sigma(T)$ increases exponentially and exhibits a broad maximum at some T_m, and then there is a region in which there is a mild decrease in $\sigma(T)$ as T increases. In metals, $d\sigma/dT < 0$, with $\sigma \propto T^{-1}$ for a simple metal, because of a temperature-dependent mobility.[35] Molecular crystals, which show a temperature region with $d\sigma/dT < 0$, are often specified as exhibiting a "metal-like" conductivity even though $\lambda/c < 1$ may obtain. This overall behavior, which we shall call type I,

contrasts sharply with the behavior (type II) of the ligand-based conductors, Ni(Pc)I[2c] and Ni(TBP)I,[2e] as well as with that of highly conductive organic materials, whose paradigm is TTF-TCNQ.[6] These typically show a broad metallic region in which $\lambda/c > 1$ and $\sigma(T) \propto T^{-\alpha}$ ($\alpha \sim 2.0$-2.5). Usually there is a relatively abrupt metal-insulator transition at some low temperature T_c.

A number of models have been proposed to explain type I conductivity behavior.[36,37] The only one which explicitly attempts to describe the full temperature response of the conductivity was proposed by Epstein and Conwell.[37] It incorporates an activation energy for a Boltzmann generation of carriers and a temperature-dependent carrier mobility $\mu \propto T^{-\alpha}$. The expression for the conductivity is

$$\sigma(T) = AT^{-\alpha} \exp(-\Delta_0/kT) \qquad (4)$$

This is the first model for type I materials which attempts to fit explicitly the whole $\sigma(T)$ curve, both below T_m in the activated region and above T_m in the metal-like region. A least-squares fit of our data for Ni(OMTBP)$(I_3)_{0.36}$ and Ni(OMTBP)$(I_3)_{0.97}$ to eq 4 yields Δ_0/k = 900 K, α = 2.87 and Δ_0/k = 1160 K, α = 2.71, respectively. The fit for the Ni(OMTBP)$(I_3)_{0.36}$ is good; the fit for the Ni(OMTBP)-$(I_3)_{0.97}$ is somewhat poorer, but this is probably a consequence of the difficulty experienced in collecting the high-temperature conductivity data for these crystals. The values of Δ_0/k and α are comparable with those observed[37] for NMP-TCNQ and Qn(TCNQ)$_2$.[6]

Although the fit of conductivities to eq 4 is good, the susceptibility results show that this model cannot describe Ni(OMTBP)$(I_3)_\rho$. The model seems to predict an activated susceptibility with a temperature dependence on the order of the gap energy, Δ_0, in contrast to the experimental observation of substantially Curie-law susceptibilities in both Ni(OMTBP)$(I_3)_\rho$ materials.

Discussion

The two Ni(OMTBP)$(I_3)_\rho$ compounds are seen to be conductive materials composed of stacks of partially oxidized macrocycles, with a ligand-centered conduction process. The more highly conducting material has a triiodide composition of ρ = 0.36, slightly higher than that of 0.33 found for the partially oxidized parent system Ni(TBP)$I_{1.0}$[2e] and the related material Ni(Pc)$I_{1.0}$.[2d] All three compounds have ML stacks separated by iodine chains. However, Ni(OMTBP)$(I_3)_{0.36}$ has a Bragg spacing between I positions of 3.77 Å, compared with values of ~3.25 Å for the others. Thus, the I chains in the crystals studied here are elongated by ~16% over those of the other materials, and could therefore have accommodated a stoichiometry of ρ = 0.39 without crowding. Failure to reach this stoichiometry suggests that beyond about ρ = 0.36 further oxidation of the macrocycle is energetically unfavorable within the particular crystal described here.

The relatively loose packing within a channel also offers a plausible reason for the greater degree of disorder found in Ni(OMTBP)$(I_3)_{0.36}$, as compared with Ni(Pc)I. It is interesting that, although appropriate random inclusion of an I_5^- rather than I_3^- could have given the same degree of oxidation, with a "filled" iodine channel, the resonance Raman spectra give no evidence for the presence of any I_5^-.

The more highly oxidized material (ρ = 0.97) discussed here must certainly adopt a different crystal structure in order to accommodate its greater iodine content. The observed g and Γ tensors have their unique axes along the needle axis, indicating respectively that the I_3^- ions lie along the needle axis and that the Ni(OMTBP) macrocycles are stacked with their normals along this needle axis. Thus the crystal also possesses stacked macrocycles and I_3^- chains just as in the ρ = 0.36 crystals, although the exact format of the stacking arrangement is not known. Perhaps the macrocycles within a stack are not rotated, opening up additional channels for iodine filling, and/or there is more than one iodine chain/channel. For these crystals the chemical analysis gives x = 2.9, not 3, and thus ρ ~ 0.97, not 1.0. Although the analytical results are not significantly different from the integral value 3.0, the essential correctness of a nonintegral x and $\rho = x/3$ is consistent with appreciable conductivity; were ρ = 1.0, then the crystal would be an integral oxidation state system and would be expected to exhibit poor conductivity. In a sense, then, the x = 2.9 crystal can be considered to be the one-electron oxidized salt of Ni(OMTBP) which has a nonintegral oxidation state by virtue of a small degree of partial reduction.

The large spacing within the Ni(OMTBP) stacks of the ρ = 0.36 material results because the exocyclic methyl groups cause severe distortion of the macrocycle. The shortest interatomic contacts between adjacent Ni(OMTBP) units are also long, 3.46 Å, compared with values of 3.25 Å in Ni(Pc)I. The poor intermolecular overlap implies that the electron transfer matrix element, t, which governs intermolecular electron transfer (the direct analogue of the Hückel β), must be much smaller than in other conductive molecular crystals. The high conductivity observed thus emphasizes the overriding importance of the nonintegral oxidation state in permitting ready charge transport.[1a,39] This importance may be understood as follows. In order to transport charge in integral oxidation state molecular systems, it is necessary to supply a large activation energy for carrier creation, since this involves high-energy states with separated positive and negative ions along a chain:

In contrast, with molecules which have been partially oxidized we have "preformed" carriers at a density of $\rho = x/3$, and we might schematically envision charge transport by a process in which "holes" move between isoenergetic configurations:

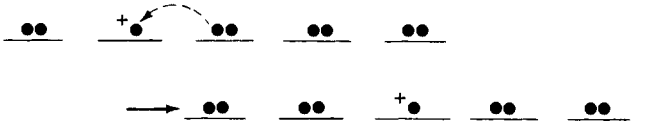

The conductivity results can be used to show[40] that for both materials the mean free path of a charge carrier is less than a lattice spacing. Thus, a picture of charge transport by diffusion of preformed carriers is appropriate, and it seems reasonable to ascribe the temperature dependence of the conductivity entirely to an activated mobility. If the EPR line width is controlled by carrier motion, this would also explain why the line width for ρ = 0.36 exhibits the same activation energy as does conductivity.

In general, the above considerations oversimplify the process of charge transport in molecular crystals. However, the observed magnetic properties of the conductive Ni(OMTBP$(I_3)_\rho$ species in fact make them different from any other well-characterized materials and demonstrate the validity of these intuitive discussions. The crux of the matter is that the susceptibility of the metal-like conductor with ρ = 0.36 shows no reduction from the Curie-law behavior expected of totally noninteracting spins and that there is only a modest reduction for ρ = 0.97. Any simple treatment of these crystals as metals would predict a low χ_e with a weak temperature dependence, while one as a semiconductor would predict an activated susceptibility.[35]

The "Hubbard model" for a one-dimensional conductor provides a conventional framework to address this problem.[41]

This model corresponds to a Hückel treatment of the linear chain with one orbital per molecule and with $\beta \leftrightarrow t$, the transfer integral as defined above. The model is extended to include a Coulomb repulsion of strength U between electrons on a given macrocycle. This parameter may be thought of as the energy required to produce separated positive and negative ions on an otherwise uncharged integral oxidation state system.

Calculations in the "atomic" limit of the Hubbard model, with finite t and $t/U \rightarrow 0$, namely, with a small but nonzero transfer integral and a large repulsion between two carriers on one site, indicate a complete decoupling of the orbital and spin degrees of freedom.[42] They predict a Curie-law susceptibility yet with high conductivity, and thus are consistent with our measurements on the $\rho = 0.36$ material; calculations[43] also correctly predict a greater degree of spin coupling for the $\rho = 0.97$ material than for $\rho = 0.36$. This limit is experimentally realized in the present materials because the large intrastack spacing reduces the overlap between the macrocycles. A detailed joint analysis of the conductivity and EPR line width[44] confirms that the temperature dependences of both quantities are wholly determined by the diffusive motion of localized carriers (polarons). Thus, the combination of properties exhibited by these materials permits the first definitive characterization of the charge-transport mechanism in a molecular metal.

In summary, the dilution effect of oxidizing "every third molecule" on a chain with already weak intermolecular coupling in fact appears to produce the situation sketched above: nondegenerate carriers are formed by oxidation, not thermal activation, and can diffuse relatively independently and rather freely, because the system energy is roughly unchanged when a carrier "jumps".

Acknowledgments. We thank Drs. Diane M. Scholler and Charles J. Schramm for assistance. One of us (B.M.H.) acknowledges Professors Z. G. Soos and A. Bloch and Dr. J. Torrance for helpful discussions. This work has been supported under the NSF-MRL program through the Materials Research Center of Northwestern University (Grant DMR76-80847 A01) and by the National Science Foundation (Grants DMR77-26409 to B.M.H. and CHE76-10335 to J.A.I.).

Supplementary Material Available: Table III, the root-mean-square amplitudes of vibration, and a table of observed and calculated structure amplitudes (4 pages). Ordering information is given on any current masthead page.

References and Notes

(1) (a) Andre, J. J.; Bieber, A.; Gautier, F. *Ann. Phys. (Paris)* **1976**, *1*, 145–256. (b) Schegolev, I. F. *Phys. Status Solidi A* **1972**, *12*, 9–45. (c) Soss, Z. G. *Annu. Rev. Phys. Chem.* **1974**, *25*, 121–152. (d) Miller, J. S.; Epstein, A. J. *Prog. Inorg. Chem.* **1976**, *20*, 1–151. (e) Keller, H. J., Ed. "Low-Dimensional Cooperative Phenomena"; Plenum Press: New York, 1975. (f) Interrante, L. V., Ed. "Extended Interactions between Metal Ions in Transition Metal Complexes", ACS Symposium Series; American Chemical Society: Washington, D.C., 1974; p 5.

(2) (a) Peterson, J. L.; Schramm, C. J.; Stojakovic, D. R.; Hoffman, B. M.; Marks, T. J. *J. Am. Chem. Soc.* **1977**, *99*, 286–288. (b) Schramm, C. J.; Stojakovic, D. R.; Hoffman, B. M.; Marks, T. J. *Science* **1978**, *200*, 47–48. (c) Hoffman, B. M.; Phillips, T. E.; Schramm, C. J.; Wright, S. K. In "Molecular Metals"; Plenum Press: New York, in press. (d) Schramm, C. J.; Scaringe, R. P.; Stojakovic, D. R.; Hoffman, B. M.; Ibers, J. A.; Marks, T. J., submitted to *J. Am. Chem. Soc.* (e) Phillips, T. E.; Pace, L.; Martinsen, J.; Hoffman, B. M.; Ibers, J. A., manuscript in preparation.

(3) Phillips, T. E.; Hoffman, B. M. *J. Am. Chem. Soc.* **1977**, *99*, 7734–7736.

(4) Teltelbaum, R. C.; Ruby, S. L.; Marks, T. J. *J. Am. Chem. Soc.* **1978**, *100*, 3215–3217.

(5) Endres, H.; Keller, H. J.; Megnamisi-Belombe, M.; Moroni, W.; Weiss, J.; Comes, R. *Acta Crystallogr., Sect. A* **1976**, *32*, 954–960.

(6) Abbreviations used: OMTBP, 1,4,5,8,9,12,13,16-octamethyltetrabenzporphyrinato; TTT, tetrathiotetracenium; Pc, phthalocyaninato; dpg, diphenylglyoximato; bqd, benzoquinonedioxamato; TPP, 5,10,15,20-tetraphenylporphyrinato; OEP, 2,3,7,8,12,13,17,18-octaethylporphyrinato; NMP, *N*-methylphenazinium; TCNQ, tetracyano-*p*-quinodimethane; Qn, quinolinium; TTF, tetrathiafulvalenium; TBP, tetrabenzporphyrinato.

(7) Bender, C. O.; Bonnett, R.; Smith, R. G. *J. Chem. Soc., Perkin Trans. 1* **1972**, 771–776.

(8) Fletcher, H. *Tetrahedron* **1966**, *22*, 2481–2486.

(9) The stoichiometry of the Ni(OMTBP)$I_{1.08}$ complex was determined both by a carbon:hydrogen analysis (1.05 ± 0.10) and from the X-ray diffraction data (1.08 ± 0.01).

(10) Shriver, D. F.; Dunn, J. B. R. *Appl. Spectrosc.* **1974**, *22*, 319–325.

(11) Phillips, T. E.; Schramm, C. J.; Anderson, J. R.; Hoffman, B. M. *Rev. Sci. Instrum.* **1979**, *50*, 263–265.

(12) Schafer, D. E.; Wudl, F.; Thomas, G. A.; Ferraris, J. P.; Cowan, D. O. *Solid State Commun.* **1974**, *14*, 347–351.

(13) Corfield, P. W. R.; Doedens, R. J.; Ibers, J. A. *Inorg. Chem.* **1967**, *6*, 197–210.

(14) The Northwestern absorption program, AGNOST, includes both the Coppens–Leiserowtiz–Rabinovich logic for Gaussian integration and the Tompa analytical method. In addition to various local programs for the CDC-6600 computer, modified versions of the following programs were employed: Zalkin's FORDAP Fourier summation program, Johnson's ORTEP thermal ellipsoid plotting program, and Busing's and Levy's ORFFE error function program. Our full-matrix, least-squares program, NUCLS, in its nongroup form, closely resembles the Busing–Levy ORFLS program. The diffractometer was run under the disk-oriented Vanderbilt system (Lenhert, P. G. *J. Appl. Crystallogr.* **1975**, *8*, 568–570.

(15) Cowie, M.; Gleizes, A.; Grynkewich, G. W.; Kalina, D. W.; McClure, M. S.; Scaringe, R. P.; Teitelbaum, R. C.; Ruby, S. L.; Ibers, J. A.; Kannewurf, C. R.; Marks, T. J. *J. Am. Chem. Soc.* **1979**, *101*, 2921–2936. Brown, L. D.; Kalina, D. W.; McClure, M. S.; Schultz, S.; Ruby, S. L.; Ibers, J. A.; Kannewurf, C. R.; Marks, T. J. *J. Am. Chem. Soc.* **1979**, *101*, 2937–2947.

(16) Euler, W. E., Pace, L., Hoffman, B. M.; Ibers, J. A., manuscript in preparation.

(17) Huml, K. *Acta Crystallogr.* **1967**, *22*, 29–37.

(18) Smith, D. L.; Luss, H. R. *Acta Crystallogr., Sect. B* **1977**, *33*, 1744–1749.

(19) Beyeler, H. U. *Phys. Rev. Lett.* **1976**, *37*, 1557–1559.

(20) Scaringe, R. P.; Ibers, J. A. *Acta Crystallogr., Sect. A* **1979**, *35*, 803–810.

(21) Warren, B. E. "X-ray Diffraction"; Addison-Wesley: Reading, Mass., 1963; p 35 ff.

(22) See paragraph at end of paper regarding supplementary material.

(23) Hoard, J. L. In "Porphyrins and Metalloporphyrins", Smith, K. M., Ed.; American Elsevier: New York, 1976; pp 328–335.

(24) Bobrovskij, A. P.; Sidorov, A. N. *J. Struct. Chem. (Engl. Transl.)* **1976**, *17*, 50–54.

(25) Atkins, P.; Symons, M. "The Structure of Inorganic Radicals"; Elsevier: Amsterdam, 1967.

(26) Dyson, F. *Phys. Rev.* **1955**, *98*, 349–358.

(27) See: Soos, Z. G.; Huang, T. Z.; Valentine, J. S.; Hughes, R. C. *Phys. Rev. B* **1973**, *8*, 993–1007.

(28) Thomas, D. D.; Keller, H.; McConnell, H. M. *J. Chem. Phys.* **1963**, *39*, 2321–2329.

(29) Hove, M. J.; Hoffman, B. M.; Ibers, J. A. *J. Chem. Phys.* **1972**, *56*, 3490–3502.

(30) A temperature-dependent single-crystal study of $\Gamma(\theta)$ was impractical as the small crystal size results in very weak signals at room temperature. Although the susceptibility increases at lower T (vide infra), qualitative microwave-power saturation measurements show that the electron spin–lattice relaxation time, T_1, increases as T decreases. This means that lower powers must be used to avoid saturation, further reducing the signal intensity.

(31) Selwood, P. W. "Magnetochemistry"; Interscience: New York, 1943; p 151.

(32) Bonner, J. C.; Fisher, M. E. *Phys. Rev. A* **1964**, *135*, 640–656.

(33) Torrance, J. B.; Tomkiewicz, Y.; Silverman, B. D. *Phys. Rev. B* **1977**, *15*, 4738–4745.

(34) We report the high-temperature behavior ($T \leq 370$ K) of the $\rho = 0.97$ composition with some caution, as the conductivity curve is not wholly reproduced upon cycling, suggesting the possibility of some crystal degradation and/or chemical reaction with the contacts. Observations of I_2 loss indicate that these crystals are stable up to 380 K and possibly 390 K, at least for ~0.5 h; I_2 is lost at 400 K, yielding crystals whose appearance is that of the $\rho = 0.36$ material.

(35) Kittel, C. "Introduction to Solid State Physics"; Wiley: New York, 1966.

(36) Bloch, A. N.; Weisman, R. B.; Varma, C. M. *Phys. Rev. Lett.* **1972**, *28*, 753–754.

(37) Epstein, A. J.; Conwell, E. M. *Solid State Commun.* **1977**, *24*, 627–630.

(38) A more recent model for the type I curves is based on the temperature-dependent gap expected for a Peierl's instability in a conducting chain: Carneiro, K. In "Molecular Metals", Hatfield, W. Ed.; Plenum Press: New York, 1979; pp 369–376. This model could also fit the overall shapes of the curves in Figure 8 with the inclusion of a temperature-dependent mobility; it would involve three fitting parameters, one for the mobility and two for the variable gap. Because of the greater complexity and flexibility of such a $\sigma(T)$ expression, we have chosen to defer application of this model until data from a variety of M(OMTBP)$(I)_x$ materials can be compared.

(39) (a) Soos, Z. G.; Klein, D. J. In "Molecular Association", Foster, R., Ed.; Academic Press: New York, 1975; Vol. I, pp 1–119. (b) Torrance, J. B. In "Chemistry and Physics of One-Dimensional Metals", Keller, H. J., Ed.: Plenum Press: New York, 1977.

(40) Mott, N. F.; Davis, E. A. "Electronic Processes in Noncrystalline Materials"; Clarendon: Oxford, 1971.

(41) Hubbard, J. *Proc. R. Soc. London, Ser. A* **1963**, *276*, 238; **1963**, *277*, 237; **1964**, *281*, 401.

(42) (a) Beni, G.; Holstein, T.; Pincus, P. *Phys. Rev. B* **1973**, *8*, 312–316. (b) Klein, D. J. *Ibid.* **1973**, *8*, 3542–3548.

(43) (a) Klein, D. J.; Seitz, W. A. *Phys. Rev. B* **1974**, *10*, 3217–3225. (b) Coll, C. F. *Ibid.* **1974**, *9*, 2150–2154.

(44) Hoffman, B. M.; Phillips, T. E.; Soos, Z. G. *Solid State Commun.* **1979**, *33*, 51–54.